JOURNAL OF CATALYSIS 121, 271–293 (1990)

Characterization of Silica-Supported Cu Monometallic and Ru–Cu Bimetallic Catalysts by Hydrogen Chemisorption and NMR of Adsorbed Hydrogen

X. WU,* B. C. GERSTEIN,† AND T. S. KING*,[1]

*Department of Chemical Engineering, 231 Sweeney Hall, and †Department of Chemistry, Iowa State University; and Ames Laboratory, Institute for Physical Research and Technology, Ames, Iowa 50011

Received March 14, 1989; revised August 17, 1989

Monometallic Ru/SiO_2 and Cu/SiO_2 catalysts and a series of $Ru–Cu/SiO_2$ bimetallic catalysts were investigated in detail by hydrogen chemisorption and nuclear magnetic resonance (NMR) of adsorbed hydrogen. NMR indicates that adsorption of hydrogen on pure Cu/SiO_2 at room temperature results in formation of a mobile, atom-like adsorbed species. Hydrogen spillover from Ru to Cu in the $Ru–Cu/SiO_2$ bimetallic catalysts was clearly shown by the two techniques. Two distinct adsorbed states of hydrogen were observed on surfaces of the Ru–Cu bimetallic particles. One state is reversibly adsorbed at room temperature while the other is irreversibly adsorbed. The reversible hydrogen exhibits rapid motion at the surface; the irreversible hydrogen is less mobile. Surface compositions for all the $Ru–Cu/SiO_2$ bimetallic catalysts were obtained from the NMR resonance lineshifts of the reversible hydrogen. The results show a preferential segregation of Cu to surfaces of Ru particles and indicate formation of large Cu islands on ruthenium and separate pure Cu particles at very high copper loadings.

INTRODUCTION

Supported Ru–Cu bimetallic catalysts (*1–14*), Ru–Cu aggregates (*15, 16*), and single-crystal Ru surfaces dosed with Cu (*17–29*) have been the frequent subjects of fundamental investigations of catalytic phenomena. Most previous investigations searched for evidence of the ensemble (or geometric) effect and electronic (or ligand) effect, suggested to be the two most important factors in interpretation of the catalytic behavior of the supported Ru–Cu bimetallic catalysts (*2*).

Ruthenium and copper are known to be immiscible in the bulk (*30*). Therefore, if there is any direct interaction between the two metals on a microscopic level, it is likely to occur at the interface. On silica-supported Ru–Cu bimetallic catalysts, Sinfelt *et al.* (*15*) proposed a microscopic model of "bimetallic clusters" with copper atoms covering the surfaces of ruthenium particles in a manner analogous to chemisorption. This model was supported later by results from extended X-ray absorption fine structure (EXAFS) (*31*). To account for the observed drop in ethane hydrogenolysis activity with increasing copper content of these supported metal catalysts, Sinfelt (*2, 4*) suggested the ensemble effect as one possible explanation.

The most studied Ru–Cu model system is the single-crystal Ru(001) surface with varying degrees of copper coverage. No convincing evidence of the ensemble effect was observed for this system catalyzing the ethane hydrogenolysis reaction (*32*). Two recent studies (*28, 33*) showed that copper forms large two-dimensional islands before completion of a monolayer. Kim *et al.* (*33*) have concluded that the model Cu/Ru(001) system could not be applied directly to the Ru–Cu aggregates and supported Ru/Cu bimetallic system because of the highly defected nature of aggregates and small particles.

Electronic interaction between ruthe-

[1] To whom correspondence should be addressed.

0021-9517/90 $3.00

nium and copper may also influence catalytic behavior. An XPS study on Ru/Cu aggregates (*16*) showed no evidence of core level electronic interactions between the two metals. A number of studies by UPS (*24, 34*) and thermal desorption of CO (*21, 24, 25, 27*) on the Cu/Ru(001) model system indicated the existence of a small electronic perturbation around the Ru–Cu interface region, probably via the valence electrons of the metals. Thermal desorption of adsorbed hydrogen from the same model systems (*26*) seemed not to be sensitive enough to show variations in binding energies associated with an electronic effect. If this electronic perturbation is significant, then the activation energies for various reactions on Ru could be altered by incorporation of Cu.

Sinfelt reported seeing no variation in activation energy for the ethane hydrogenolysis reaction when copper is added to silica-supported ruthenium (*2*). Similarly, Bond and Turnham (*11*), studying CO hydrogenation, found the activation energy to be invariant with copper content. On the other hand, Lai and Vickerman (*13*) did see a variation in activation energy for the CO hydrogenation reaction. Recent work in our laboratories that used chlorine-free Ru–Cu/SiO_2 catalysts also indicated variations in activation energies for the ethane hydrogenolysis reaction (*35*).

To clearly distinguish between ensemble and electronic effects (if they exist) and to interpret catalytic results properly, one must know the amount of active metal (in this case ruthenium) available at the surface. Hydrogen chemisorption has been used to titrate the amount of Ru at the surface in the Ru–Cu bimetallic system. The method is based on the assumption that copper does not dissociatively adsorb molecular hydrogen, and it seems to be true for single-crystal Cu surfaces where adsorption of molecular hydrogen is an activated process with an activation energy of about 5 kcal/mol (*36, 37*). However, conflicting results on the influence of Cu in hydrogen chemisorption capacity of Ru have been reported on silica-supported Ru–Cu catalysts. Sinfelt *et al.* (*2, 4, 15*) reported a suppression of hydrogen chemisorption by Cu while Haller and co-workers (*5, 6*) found no significant influence of Cu on the hydrogen chemisorption capacity of ruthenium. This latter finding was attributed to spillover of atomically adsorbed hydrogen from ruthenium sites to adjacent copper sites after dissociative adsorption of molecular hydrogen on ruthenium. Recent studies (*38, 39*) on the Cu/Ru(001) model system also revealed such a hydrogen spillover phenomenon at temperatures above 230 K. This view was later supported by an NMR study on hydrogen chemisorbed on Ru–Cu/SiO_2 catalysts at room temperature (*40*). These results confirmed the spillover of hydrogen from ruthenium to copper on supported Ru–Cu bimetallic catalysts.

With only a few exceptions (*5–7*) the ruthenium salt $RuCl_3 \cdot nH_2O$ has been used as a precursor in preparing Ru–Cu/SiO_2 catalysts in previous investigations. The effect of chlorine contamination on the hydrogen chemisorption capacity of Ru has been overlooked until recently. A number of studies (*41–43*) indicated that a substantial amount of chlorine remains on the surfaces of ruthenium particles after reduction at normal reduction temperatures (573–773 K), and the residual chlorine inhibits adsorption of hydrogen on ruthenium. Recent results in the authors' laboratory have supported this picture (*44*). If the incorporation of Cu further inhibits the reducibility of $RuCl_3$, then one may observe an apparent suppression of hydrogen chemisorption capacity upon addition of copper. The introduction of chlorine complicates the characterization of Ru/SiO_2 and Ru–Cu/SiO_2 catalysts by hydrogen chemisorption. The inability to characterize these catalysts cast doubt upon the interpretations of reaction data obtained from these catalysts in the previous investigations.

The objectives of the present study were to reexamine the phenomenon of hydrogen

spillover from Ru to Cu and to determine the overall surface compositions of the Ru–Cu bimetallic particles on clean Ru–Cu/SiO_2 catalysts by means of hydrogen chemisorption and nuclear magnetic resonance of adsorbed hydrogen.

EXPERIMENTAL

Catalysts Preparation

The Ru/SiO_2 and Cu/SiO_2 catalysts were prepared by incipient wetness impregnation of a ruthenium or copper impregnating solution with a dried Cab-O-Sil HS5 (300 m^2/g BET surface area) silica support. The Ru–Cu/SiO_2 catalysts were prepared by coimpregnation of a ruthenium–copper impregnating solution in the same manner. The impregnating solutions were prepared by dissolving either $Ru(NO)(NO_3)_3$ salt (AESAR) or $Cu(NO_3)_2 \cdot 6H_2O$ (AESAR, 99.999%) or both in distilled water. About 2.2 ml of impregnating solution per gram of SiO_2 was sufficient to bring about incipient wetness. The slurries obtained after impregnation and mixing were dried for 24 h at room temperature and 4 h in air at 383 K. The ruthenium loading for all ruthenium-containing catalysts was kept at 4% by total weight of the support and metals. The copper loading for the Cu/SiO_2 catalyst was 5%. A total of 10 different Ru–Cu/SiO_2 catalysts was prepared to give a wide range of copper loading. The amount of copper in each Ru–Cu/SiO_2 catalyst and the Cu/SiO_2 catalyst was determined by atomic absorption spectroscopy.

Volumetric Adsorption Apparatus

The adsorption apparatus was a multiport Pyrex glass manifold 127.3 cm^3 in volume connected to a high-vacuum system, which included a turbo-molecular pump (Balzers, Model TPH050), a fore-pump trap, and a two-stage mechanical pump. The apparatus was designed to have a flow-through capability for reduction of catalyst samples. High-vacuum greaseless, bakeable stopcocks (Ace Glass) with Teflon plugs and FETFE o-ring seals were employed to manipulate gas storage, dosage, or both and to eliminate hydrocarbon contamination in the manifold. The manifold was capable of a vacuum better than 10^{-7} Torr (1 Torr = 133.3 Pa) after bakeout. Pressures below 10^{-2} Torr were monitored by a cold cathode vacuum gauge (Varian, Model 860A). Pressures from 0.01 to 1000 Torr were measured by two absolute Baratron pressure gauges (MKS).

A flow-through Pyrex cell mounted with a coarse glass frit (35 μm in average pore diameter) was used to contain catalyst samples for the volumetric adsorption experiments. A small furnace was used to provide uniform heating to the cell. The temperature inside the furnace was controlled by a proportional temperature controller (Omega) to within ± 1 K.

Catalyst Reduction and Volumetric Adsorption

Approximately 1 g of a catalyst sample was loaded into the flowthrough cell, which was then attached to one of the sample ports of the manifold. The temperature around the cell was raised to 423 K while helium gas flowed through the sample bed in the cell. Then helium was switched off and replaced by hydrogen gas at a flow rate of 50 cm^3/min. A prereduction period of 1 h proceeded at that temperature. The temperature was then raised at 10 K/min to 723 K. Further reduction was carried out for 2 additional h at 723 K. Helium (99.999%) and hydrogen (99.8%) gases (Liquid Air Co.) were used as received. The sample was then evacuated for 2 h at 723 K to remove traces of water and surface hydrogen. The reduction temperatures used for the 5% Cu/SiO_2 catalyst was 623 K.

Hydrogen for volumetric adsorption and dosage on NMR samples was purified by passing it through a catalytic hydrogen purifier (Engelhard Deoxo) in series with a gas purifier with Drierite and a 5-Å molecular sieve (Alltech) to remove traces of oxygen and moisture. Hydrogen adsorption experi-

ments were performed at ambient temperature (294 K). The total hydrogen adsorption isotherm was measured in the pressure range of 0–60 Torr. The reversible hydrogen adsorption isotherm was measured under the same conditions after a 10-min evacuation to a pressure of 10^{-6} Torr following the total adsorption. The irreversible hydrogen uptake was obtained by taking the difference between the extrapolated values of the total and the reversible isotherms at zero pressure. Equilibration times used were 4 h for the first dose and 1 h for subsequent doses.

NMR Sample Treatment

A specially designed stainless-steel needle and bellows assembly was used for direct reduction of a catalyst sample in flowing hydrogen inside a 5-mm NMR tube. The syringe needle (18 gauge) was capable of moving vertically by more than 6 cm through adjustable compression and extension of the bellows. Vacuum-tight connections were made between the NMR tube and the needle and bellows assembly and also between the assembly and the manifold described above. In addition, a small cylindrical furnace provided uniform heating around the NMR tube, and the temperature of the furnace was controlled to within 1 K.

With helium gas flowing through the needle, the needle was lowered to the bottom of the NMR tube containing approximately 60 mg of catalyst sample. The reduction procedure was the same as that previously described for the volumetric adsorption experiment, with a hydrogen flow rate of 15 cm^3/min. After reduction, the needle was elevated out of the sample, and evacuation proceeded for 2 at the reduction temperature before the sample was allowed to cool to ambient temperature. Up to four samples could be reduced simultaneously. Purified hydrogen was then dosed through the needle to each sample separately, and the system was allowed to equilibrate for 4 h. The NMR tube containing the sample was then immersed in a water bath and was sealed off with a microtorch. The sample weight was measured after the NMR tube was sealed. For the deuterium exchange experiment, deuterium gas (Linde, 99.5%) instead of hydrogen was used as the adsorbate.

NMR EXPERIMENTS

The home-built NMR spectrometer (*45*) used for the present study was operated at 220 MHz for proton resonance. A proton-free probe with a doubly wound coil (*46*) was used for all the NMR measurements. The probe quality factor Q was set at about 100 to obtain the optimal values of sensitivity and ringdown time for a fixed pulse power (*47*). A detailed description of the spectrometer's rapid-recovery receiving system has been published elsewhere (*48*).

All NMR spectra collected were under a repetitive 90° single-pulse sequence. The recycle time between rf pulses was set at 0.2 s to selectively suppress the strong intensity of the peak corresponding to protons in the silanol group in the silica support, which has a relatively long spin–lattice relaxation time T_1 (on the order of seconds). This repetition rate avoids T_1 saturation on all peaks corresponding to hydrogen adsorbed on ruthenium and copper. The total number of scans for data acquisition on each sample was 10,000. The inversion recovery pulse sequence (180°–τ–90°) was applied to measure the spin–lattice relaxation times of both the silanol protons (in the time domain) and the hydrogen adsorbed on metals (in the frequency domain). A pure water sample was used as the reference standard for the observed lineshifts.

For spin counting, the water reference was doped with $FeCl_3$ to yield a resonance of a comparable linewidth with the observed resonances. The doped water was sealed in a capillary tube that had the same length as the catalyst sample in the NMR tube to offset errors due to B_1 inhomogeneity in the coil. All NMR measurements were taken at ambient temperature (294 ± 1 K).

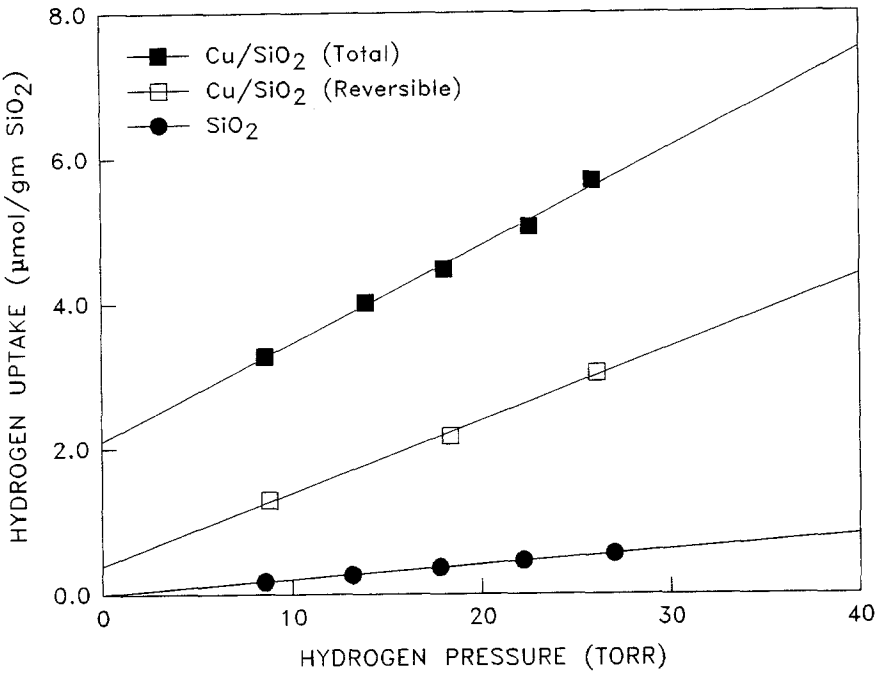

FIG. 1. Hydrogen adsorption isotherms (294 K) measured by the volumetric technique on a pure SiO_2 sample and a 5% Cu/SiO_2 catalyst.

RESULTS

The amount of hydrogen adsorbed on a pure SiO_2 sample treated in the same way as a silica-supported catalyst was measured. The results shown in Fig. 1 indicate there is a very small amount of adsorbed hydrogen on pure SiO_2 in the hydrogen pressure range of 5 to 30 Torr. However, a linear extrapolation of the adsorption isotherm to zero hydrogen pressure yields no hydrogen uptake. Consequently, hydrogen adsorption by the support has no contribution in similar measurements on silica-supported metal catalysts.

The volumetric technique applied to the 5% Cu/SiO_2 catalyst indicated that there was hydrogen adsorption by copper, as shown also in Fig. 1. By linear extrapolation of either the total or the reversible isotherm to zero pressure, it is clear that a small amount of chemisorbed hydrogen exists on copper. On the same basis, this hydrogen uptake was less than 3% of that for a 4% Ru/SiO_2 catalyst (shown later). The dispersion of the 5% Cu/SiO_2 catalyst was about 0.06 as measured by nitrous oxide adsorption (*49*).

NMR of adsorbed hydrogen on the 5% Cu/SiO_2 catalyst yielded similar results. As shown in Fig. 2, NMR spectra of hydrogen adsorbed on a 5% Cu/SiO_2 sample display two distinct resonance lines. The resonance line near the reference shift position (4 ± 1 ppm) was identified as the proton in the silanol group (Si–OH) in the silica support. Only this resonance line appeared for samples of pure SiO_2 either under vacuum or under 30 Torr hydrogen gas. The resonance line downfield to that of the silanol proton was assigned to hydrogen adsorbed on pure copper surfaces. For the Cu/SiO_2 sample under 30 Torr hydrogen gas, the position of the downfield peak is at -93 ppm, and the peak displays a sharp feature with a linewidth (full width at half maximum) of about 730 Hz. A similar shift value for hydrogen adsorbed on a copper powder relative to an

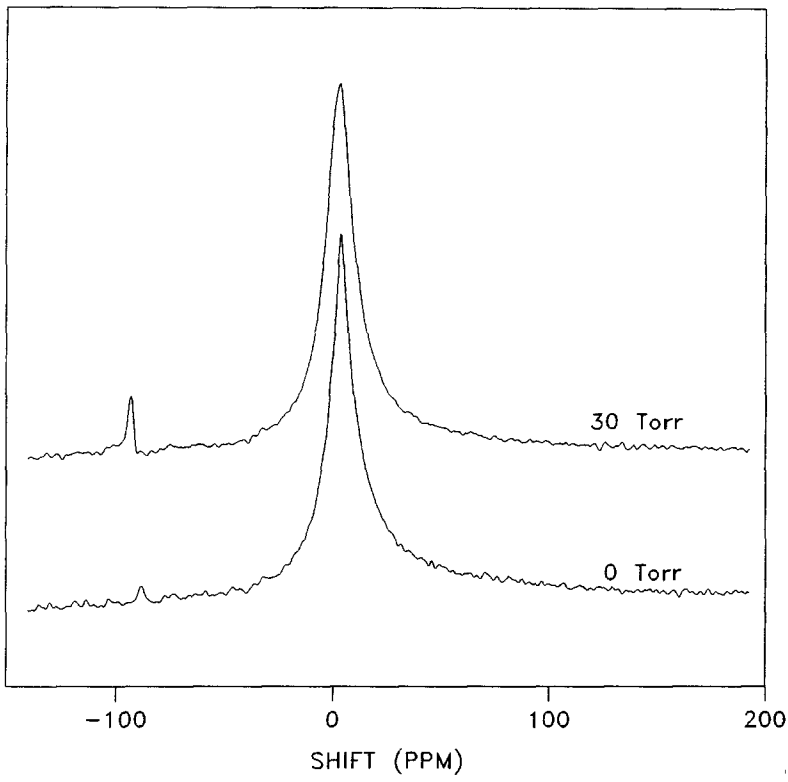

FIG. 2. NMR spectra of adsorbed hydrogen on a 5% Cu/SiO_2 catalyst. Hydrogen pressures are as indicated. "0 Torr" denotes an evacuation condition of 10^{-6} Torr for 10 min at 294 K after adsorption under 30 Torr hydrogen. Water is used as a reference for the lineshift.

unknown reference has been reported (*50*). When the Cu/SiO_2 sample is evacuated to 10^{-6} Torr for 10 min after dosage of 30 Torr hydrogen gas, the downfield peak is diminished in intensity but still observable. Its position has moved from −93 to −88 ppm. The amount of adsorbed hydrogen determined by proton spin counting via NMR agrees roughly with volumetric adsorption measurements.

The H/Cu ratio is about 10% of what would be expected from a complete coverage of hydrogen at the measured copper dispersion. In other words, only 10% of the surface copper atoms are capable of adsorbing hydrogen. This result agrees with results from studies on bulk Cu surfaces (*50–52*) which also show low coverages by hydrogen.

In Fig. 3 is shown a single NMR spectrum of a mixture of Cu/SiO_2 and Ru/SiO_2 under 30 Torr hydrogen gas. The physical mixture was prepared by mechanically mixing an approximately equal amount of the reduced 4% Ru/SiO_2 and 5% Cu/SiO_2 catalysts. The mixture was then reduced again at 623 K for 1 h. The sample prepared in this manner should contain only separate Ru and Cu metal particles. As shown in Fig. 3, two well-separated resonance lines other than the silanol proton resonance line were observed. The upfield peak relative to the silanol proton peak was located at +62 ppm and had a relatively intense resonance signal. This upfield peak is identified as the resonance of hydrogen adsorbed on pure ruthenium surfaces (*53*). The intensity of the downfield peak (−93 ppm), associated

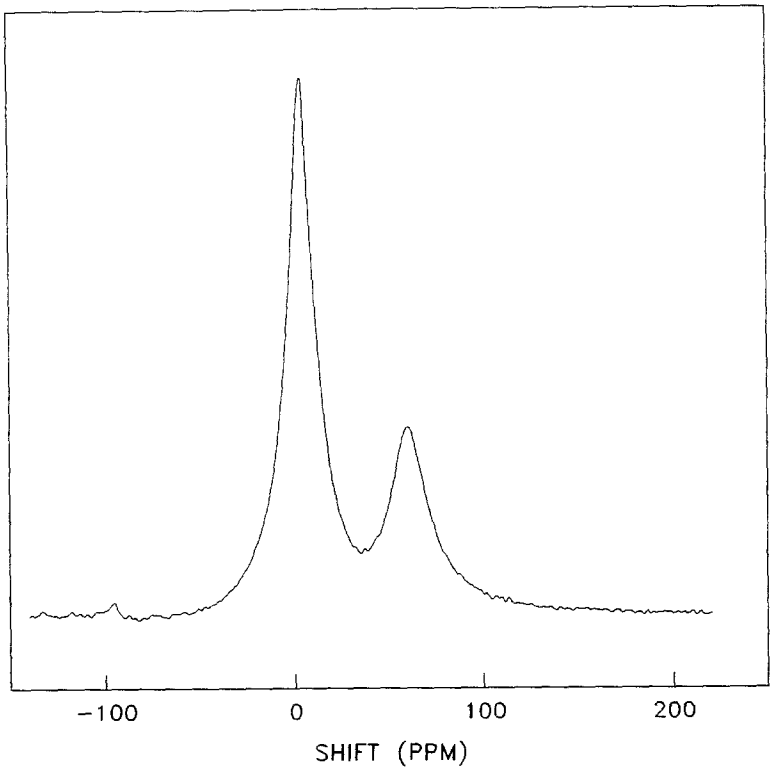

FIG. 3. An NMR spectrum on a Ru/SiO_2 + Cu/SiO_2 physical mixture under 30 Torr hydrogen. The mixture contains approximately equal amounts of a 4% Ru/SiO_2 and a 5% Cu/SiO_2 catalyst.

with hydrogen adsorbed on copper, was relatively weak. The spectrum clearly confirmed the existence of only separate pure Ru and Cu particles in the Ru/Cu physical mixture.

A set of NMR spectra for the 4% Ru/SiO_2 catalyst and the 4% Ru–Cu/SiO_2 catalysts with a wide range of copper loading is shown in Fig. 4. The copper content is given as an atomic percent of the total metal present in a given catalyst. NMR of ^1H on all catalyst samples was obtained with the sample under 60 Torr hydrogen gas. As expected for the Ru/SiO_2 catalyst, a distinct resonance line corresponding to hydrogen adsorbed on ruthenium appeared at +61 ppm upfield of the reference (*53*). Three interesting features developed as the copper loading was increased: (1) the position of the upfield peak moved downfield toward the silanol proton peak with an increase in the copper loading; (2) the linewidth of the upfield peak became broadened and its intensity lowered as the copper loading was increased, and the combined effect of these two trends resulted in a reduced spectral resolution due to increased overlap between the upfield peak and the silanol proton peak; and (3) a peak became visible downfield of the silanol proton peak, at copper bulk compositions of about 45 at.% and higher. The downfield peak intensity was increased with an increase in the copper loading. Also, there was a small upfield shift of the downfield peak with an increase in the copper loading.

The silanol proton peak has a symmetric lineshape. The upfield peak is asymmetric. The upfield peak can be deconvoluted by subtracting the silanol proton peak from the

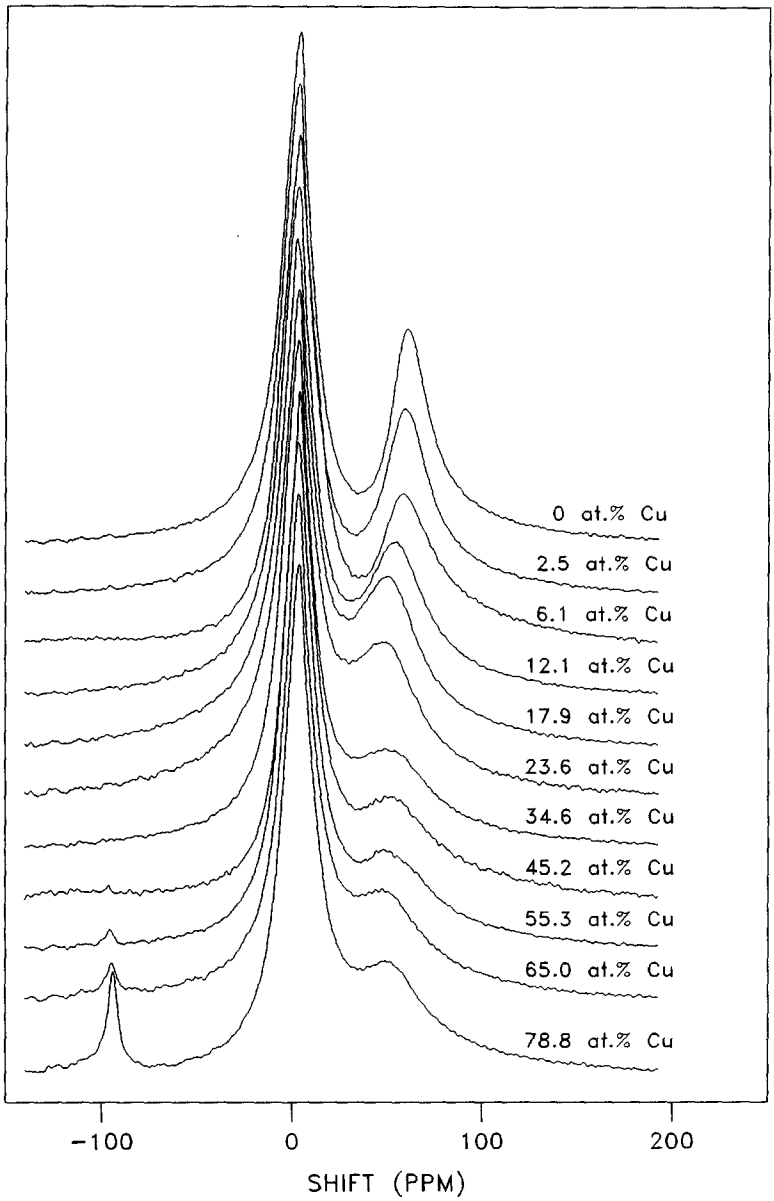

FIG. 4. NMR spectra of adsorbed hydrogen on a series of Ru–Cu/SiO_2 bimetallic catalysts under 60 Torr hydrogen. The copper bulk compositions expressed as atomic percent are as indicated.

spectrum. The intensity of the upfield peak can then be obtained by integrating the area under the deconvoluted upfield peak. The location of the upfield peak is taken to be the first moment of the deconvoluted resonance line.

The changes of the upfield peak position and resonance linewidth with variation in the copper loading are clearly an effect solely due to incorporation of copper because the Ru loading and the hydrogen pressure are kept constant for all the catalyst samples. As shown earlier in Fig. 3, the resonance position and linewidth of the upfield peak corresponding to hydrogen adsorbed on pure Ru surfaces is not affected

by physically mixing Cu/SiO_2 with Ru/SiO_2. This result indicates that copper and ruthenium do come together to form Ru–Cu bimetallic particles upon reduction of the coimpregnated $Ru–Cu/SiO_2$ materials.

The positions of the downfield peak for $Ru–Cu/SiO_2$ catalysts with a copper composition greater than 45 at.% were in the range of −93 to −97 ppm. The assignment of this downfield peak to hydrogen adsorbed on pure copper surfaces was reasonable because we observed a similar lineshift on a pure Cu/SiO_2 catalyst sample (Fig. 2). The emergence of this peak may indicate the formation of large Cu islands on the Ru–Cu bimetallic particles or buildup of separate copper particles.

Figure 5 shows a set of NMR spectra for the 4% Ru/SiO_2 catalyst and six 4% $Ru–Cu/SiO_2$ catalysts having various copper loadings. All catalyst samples were evacuated to 10^{-6} Torr for 10 min after adsorption with 60 Torr hydrogen. Obviously, the upfield peak corresponding to the irreversibly adsorbed hydrogen on surfaces of pure Ru or Ru–Cu bimetallic particles exhibits an asymmetric resonance line that is considerably broader than the upfield peak under 60

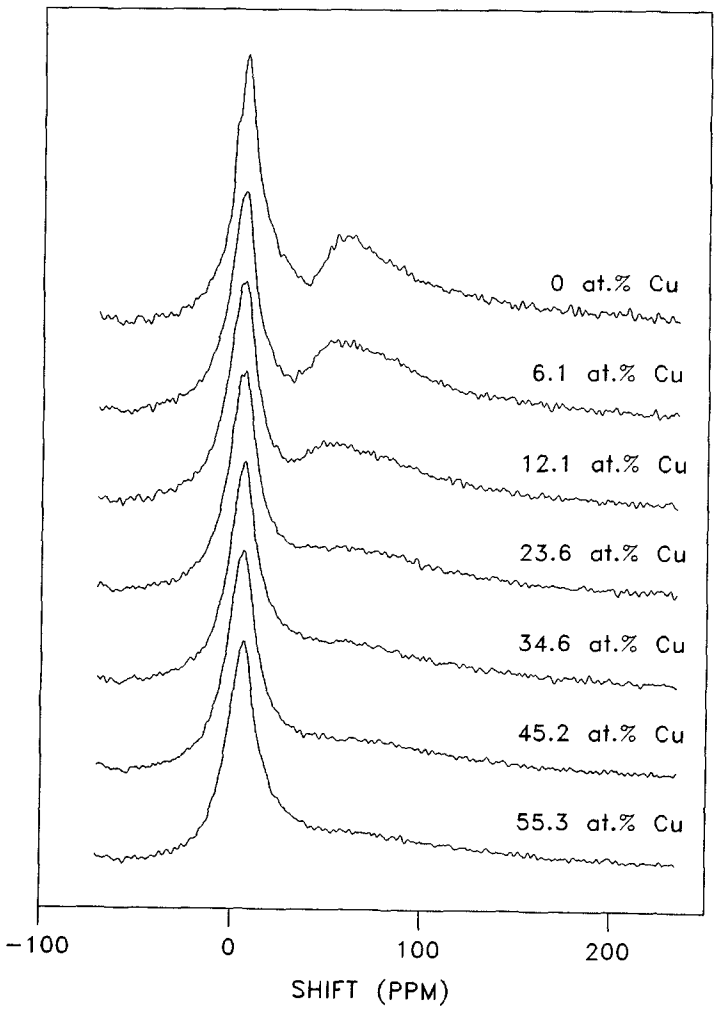

FIG. 5. NMR spectra of the irreversibly adsorbed hydrogen on a series of $Ru–Cu/SiO_2$ bimetallic catalysts. The copper bulk compositions expressed as atomic percent are as indicated.

Torr hydrogen (see Fig. 4). While the intensity of this peak decreases with an increase in the copper loading, its linewidth increases from 10.9 kHz for the pure Ru/SiO_2 sample to 22.6 kHz for the Ru–Cu bimetallic sample having a bulk copper composition of 55.3 at.%. No resonance signals downfield from the silanol proton peak were observed for all the catalysts shown in this figure. However, we did observe a very weak resonance signal downfield of the silanol proton peak for a $Ru–Cu/SiO_2$ bimetallic catalyst sample with a bulk copper composition of 78.8 at.% (not shown in Fig. 5). This NMR spectrum will be shown later along with other spectra of the same catalyst under various hydrogen pressures.

The asymmetry of the upfield peaks shown in Fig. 4 was caused by the asymmetric feature of the upfield peaks corresponding to the irreversible hydrogen as shown in Fig. 5. As indicated in previous investigations on a number of pure Ru/SiO_2 catalysts, the spectral asymmetry for samples under 5 Torr hydrogen may be removed simply by subtracting the corresponding resonance line for the irreversible adsorption from the observed spectra (*53*). The result is a near-symmetric resonance resembling a Lorentzian line that corresponds to the reversibly adsorbed hydrogen on ruthenium. The same approach was applied here for all the $Ru–Cu/SiO_2$ bimetallic catalysts by subtracting the resonance line for the irreversibly adsorbed hydrogen from that corresponding to the same catalyst under 60 Torr hydrogen. The resulting difference spectra were indeed nearly symmetric and were much narrower. The linewidth was in the range of 3.6 to 8.9 kHz compared to 10.9 to 24.0 kHz for the irreversible hydrogen, with the pure Ru/SiO_2 catalyst having the narrowest linewidth. This spectral narrowing is an indication of a higher degree of mobility for the reversibly adsorbed than for the irreversibly adsorbed hydrogen.

In both Figs. 4 and 5, the upfield peak-integrated intensity decreased with an increase in copper content. The apparent decrease in the upfield peak intensity in both cases was associated with line broadening of the irreversibly adsorbed hydrogen with addition of copper. The loss of intensity is caused by the increased loss of initial intensity due to receiver ring-down in the time domain. The relative intensity of the upfield peak corresponding to the reversible hydrogen as measured from the difference spectrum remains roughly the same for all the Ru/SiO_2 and $Ru–Cu/SiO_2$ samples.

The intensity measurements for the upfield peak were performed on all the Ru/SiO_2 and $Ru–Cu/SiO_2$ catalysts under various hydrogen pressures ranging from 5 to 60 Torr. Similar to what was observed on numerous pure Ru/SiO_2 catalysts (*53*), isotherms obtained in this manner exhibit nearly straight lines over this hydrogen pressure range. The slopes of these isotherms match closely those obtained by the volumetric method of hydrogen chemisorption. All isotherms were extrapolated to zero hydrogen pressure to obtain values of the H/Ru ratio. The dependence of the upfield peak intensity with the hydrogen pressure indicates that more reversibly adsorbed hydrogen is present on surfaces of Ru and Ru–Cu particles under higher hydrogen pressure.

The values of the H/Ru ratio (extrapolated to zero pressure) for the total and the irreversible hydrogen adsorption as measured by both hydrogen chemisorption and NMR of adsorbed hydrogen are shown in Fig. 6 as functions of atomic percent copper. Contrary to that reported by Sinfelt (*2*), perhaps due to different catalyst precursors used, addition of copper to ruthenium does not suppress the hydrogen chemisorption capacity in cases of both the total and the irreversible adsorption as measured by the volumetric technique. Rather, it slightly enhances the capacity for hydrogen chemisorption. This observation agrees with the results reported by Haller and co-workers (*5*). The apparent hydrogen chemisorption capacity measured by the

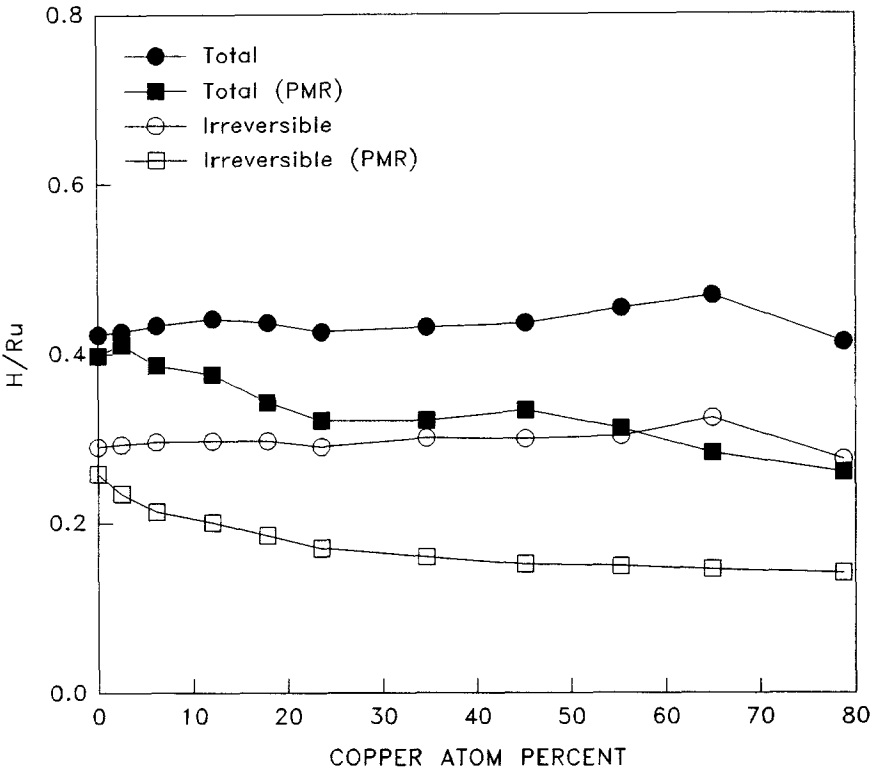

FIG. 6. The H/Ru ratios for both the total and the irreversible adsorption of hydrogen on a series of Ru–Cu/SiO_2 bimetallic catalysts. Results from measurements by both the volumetric technique and ^1H NMR are shown for comparison.

upfield peak intensity from the NMR spectrum decreases with the addition of copper. This apparent loss of intensity is due to the increasingly broad spectral features as shown in Figs. 4 and 5. However, the chemisorption capacity for the reversible hydrogen (taken as the difference between the total and the irreversible adsorption) remains almost unchanged for all the Ru/SiO_2 and Ru–Cu/SiO_2 catalysts as measured by both volumetric technique and NMR of adsorbed hydrogen.

The effect of copper content on the location of the upfield resonance line has been illustrated earlier in Fig. 4. The numerical values of this lineshift as calculated by the first moment as a function of copper content are shown in Fig. 7. Also shown in the figure are the shifts in first moment for the reversibly adsorbed hydrogen obtained from the difference spectra between the NMR spectra under 60 Torr hydrogen and the corresponding NMR spectra for the irreversible hydrogen. The results in Fig. 7 indicate that the first moment of the resonance for the reversibly adsorbed hydrogen is slightly upfield relative to the peak corresponding to all the hydrogen adsorbed at 60 Torr on the Ru/SiO_2 and Ru–Cu/SiO_2 catalysts. For both the reversible and the total hydrogen, a similar trend for the lineshift as a function of copper content was observed. A relatively large change in the upfield peak lineshift occurred at copper bulk compositions between 0 and 20 at.%. Further increase in the copper content resulted in only a small decrease in the lineshift. Although the shifts in resonance for the irreversible hydrogen are not shown, they are slightly further downfield than those under

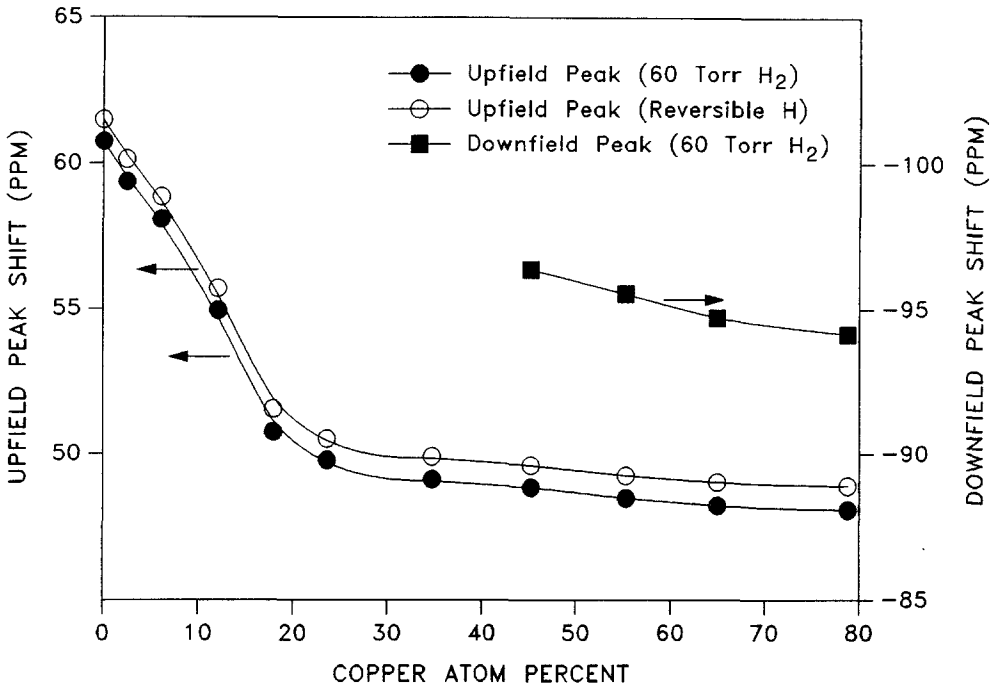

FIG. 7. Variations of both upfield and downfield lineshifts under 60 Torr hydrogen with the copper composition for Ru–Cu/SiO_2 bimetallic catalysts. Upfield lineshifts for the reversible hydrogen are also shown.

60 Torr hydrogen and exhibit the same trend as a function of the copper content. The shift associated with the irreversibly adsorbed hydrogen is not shown because the line broadening due to addition of copper makes the exact location of the resonance line for the irreversible hydrogen difficult to determine, especially at high copper content.

The shifts of downfield peak (assigned to hydrogen adsorbed on copper) are also plotted in Fig. 7 as a function of the copper content. A small change in the shift was observed over the range of copper bulk compositions from 45 to 79 at.%. The trend of this peak's shift toward upfield with increase in the copper content may be an indication of subtle changes in adsorption properties of surface copper sites due to variations in copper particle size. The increase in copper particle number and size with increase in the copper content was indicated by the increase in the signal intensity of the hydrogen adsorbed on copper as shown earlier in Fig. 4.

Over 95% of the total hydrogen population in all catalyst samples investigated in the present study comes from protons in the silanol group. Therefore, measurements on the spin–lattice relaxation time T_1 of the silanol proton can be performed in the time domain with the inversion recovery pulse sequence, and the influence by the proton population on the metal(s) can be neglected. Exponential profiles were obtained in plots of the measured magnetization versus the delay time, τ, for samples of a pure SiO_2 and a reduced 4% Ru/SiO_2 in the absence of dosed hydrogen. The measured T_1's for these two samples were 31.6 and 16.9 s, respectively. Small deviations from the exponential were observed for all Ru/SiO_2 and Ru–Cu/SiO_2 catalyst samples in the presence of dosed hydrogen due to the

relaxation effect from hydrogen spillover to the silica support, as discussed in the case of Ru/SiO_2 (*53*). Nevertheless, the same method was applied to obtain a single T_1 value for each of these samples.

Figure 8 shows variation with the copper content of the T_1 for the silanol protons. The results for samples under 60 Torr hydrogen and for samples evacuated to 10^{-6} Torr for 10 min after equilibrium with 60 Torr hydrogen are shown. For all samples under 60 Torr hydrogen, the spin–lattice relaxation time remains essentially unchanged at about 2.5 s. For the evacuated samples, there was a moderate decrease in T_1 as the copper content was increased.

The spin–lattice relaxation time for hydrogen adsorbed on the metals was measured in the frequency domain by using inversion recovery. The initial magnetizations were obtained indirectly by integrating the area of the resonance line corresponding to hydrogen adsorbed on Ru, Cu, or Ru–Cu. A linear regression of the log of this area versus delay time for each sample yielded the values of T_1.

The value of T_1 of hydrogen chemisorbed on Ru/SiO_2 and Ru–Cu/SiO_2 (the peak farthest upfield) was determined under two conditions: under 60 Torr hydrogen and after evacuation to 10^{-6} Torr for 10 min following exposure to 60 Torr hydrogen (irreversibly adsorbed hydrogen). The results are shown in Fig. 9. Note that the irreversibly adsorbed hydrogen has a longer T_1 than that of the hydrogen corresponding to the irreversibly plus reversibly adsorbed hydrogen. The addition of copper tends to increase the T_1 value. Because of the above-mentioned line-broadening effect by copper, the exact values of T_1 for the irreversibly adsorbed hydrogen at bulk compositions greater than 35 at.% Cu were difficult to determine. However, they seemed to follow the same trend as those under 60 Torr hydrogen.

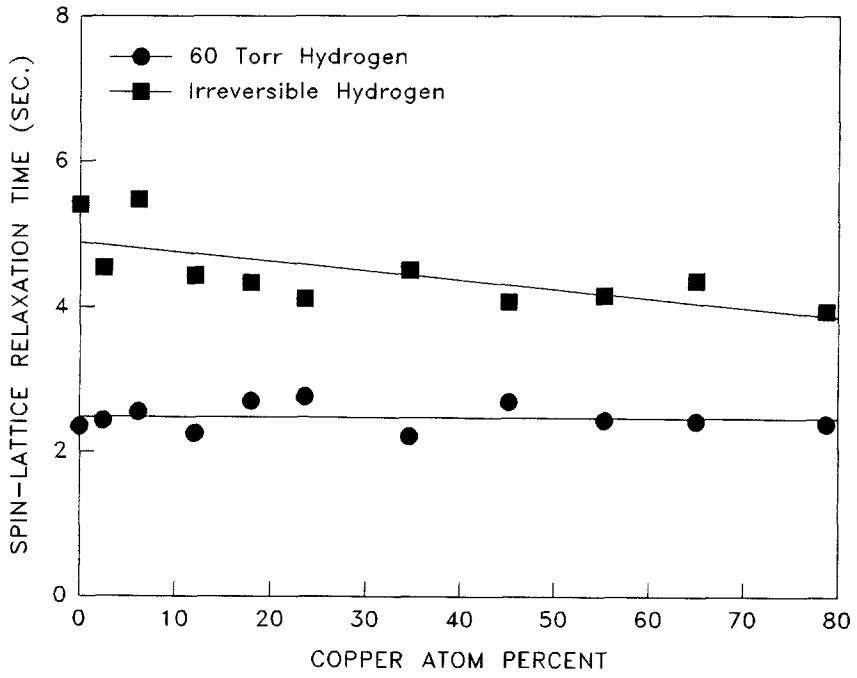

FIG. 8. Variations of spin–lattice relaxation times of the silanol proton with the copper composition for Ru–Cu/SiO_2 bimetallic catalysts. Results for both 60 Torr hydrogen and the irreversible hydrogen are shown.

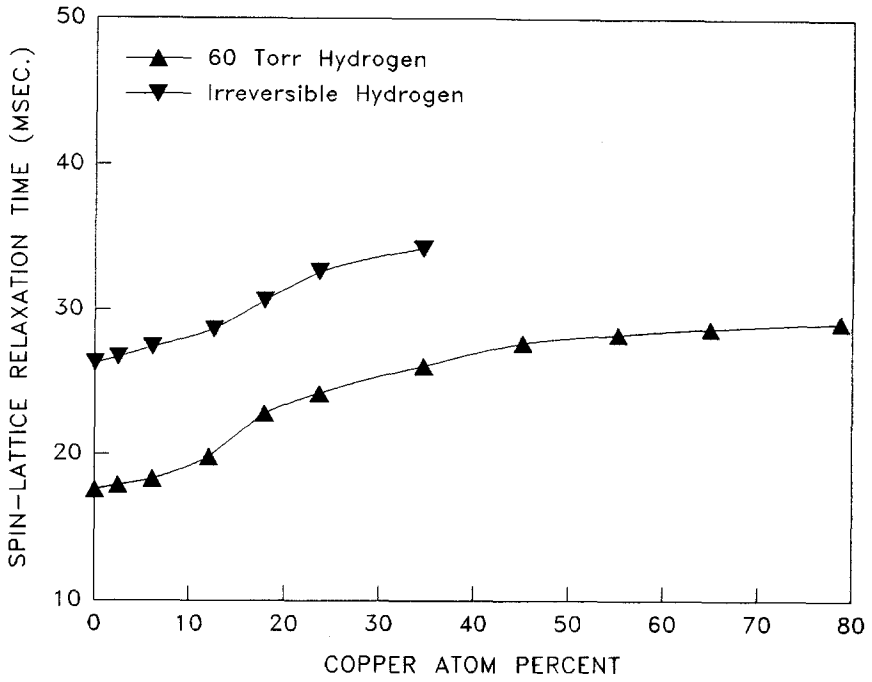

FIG. 9. Variations of spin–lattice relaxation times of the upfield peak with the copper bulk composition for Ru–Cu/SiO_2 bimetallic catalysts. Results for both 60 Torr hydrogen and the irreversible hydrogen are shown.

The proton NMR spectra of hydrogen on Ru–Cu/SiO_2 with the highest copper loading (78.8 at.% Cu) under various hydrogen pressures are shown in Fig. 10. The spectrum denoted as "0 Torr" represents a catalyst sample evacuated to 10^{-6} Torr for 10 min after exposure to 60 Torr hydrogen. Some obvious spectral features can be readily seen. First, the signal intensities of both the upfield peak and the downfield peak relative to the silanol proton peak increase with increasing hydrogen pressure. Secondly, both upfield and downfield peaks exhibit some degree of line narrowing as the hydrogen pressure is increased. The linewidths for the upfield peak are comparable to those reported earlier, namely about 8 kHz under 120 Torr hydrogen and about 24 kHz under the evacuation condition. The linewidths for the downfield peak decrease from 3.9 kHz under 5 Torr hydrogen to 2.3 kHz under 120 Torr hydrogen. The third feature is a notable downfield shift of the downfield peak as the hydrogen pressure is increased. These observations indicate a buildup of the highly mobile, reversibly adsorbed hydrogen on the surfaces of the metal particles as the hydrogen pressure is increased.

The relative signal intensities (normalized to those under 120 Torr hydrogen) for both the upfield and the downfield peak and also the lineshift for the downfield peak are plotted in Fig. 11 versus the hydrogen pressure. The relative intensities for the two peaks follow roughly the same trend as the hydrogen pressure is increased. Note that there is a strong dependence of the amount of reversibly adsorbed hydrogen on hydrogen pressure. Also, the intensities over the hydrogen pressure range of 5 to 60 Torr fall approximately on a straight line in both cases.

For the same Ru–Cu/SiO_2 catalyst (78.8 at.% Cu), the spin–lattice relaxation times on the silanol peak, the upfield peak, and

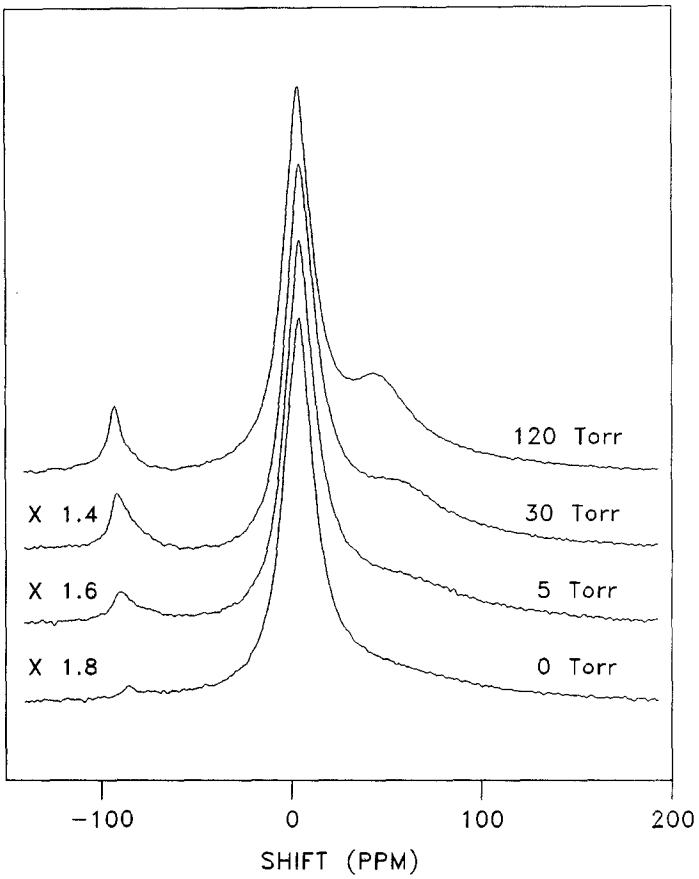

FIG. 10. NMR spectra of adsorbed hydrogen on a Ru–Cu/SiO_2 bimetallic catalyst with 78.8 at.% Cu under various hydrogen pressures. The hydrogen pressures are as indicated. "0 Torr" denotes an evacuation condition of 10^{-6} Torr for 10 min at 294 K after adsorption under 60 Torr hydrogen.

the downfield peak were measured by the methods mentioned earlier. The results are shown in Fig. 12 as functions of the hydrogen pressure. As expected, the T_1 of the silanol proton exhibited a decrease from 4 to 1.8 s over the hydrogen pressure range of 0 to 120 Torr because of increased hydrogen spillover from the metals to SiO_2. This higher degree of hydrogen spillover is a direct consequence of increased adsorption of the reversible hydrogen on the metals. The T_1's of hydrogen adsorbed on the metals exhibited nearly identical numerical values for both the upfield and the downfield peak and the same decreasing trend with increasing hydrogen pressure.

Hydrogen–deuterium exchange experiments were performed on the Ru–Cu/SiO_2 catalyst with the highest copper loading (78.8 at.% Cu) and the 5% Cu/SiO_2 catalyst. For the Ru–Cu/SiO_2 catalyst, the exchange was monitored under two conditions: under 60 Torr deuterium and after evacuation to 10^{-6} Torr for 10 min following exposure to 60 Torr deuterium. As clearly shown in spectrum A in Fig. 13, deuterium adsorbed on surfaces of the Ru–Cu bimetallic and Cu particles does exchange with the silanol protons in the silica support under 60 Torr deuterium. This is evident by the growth of the upfield and the downfield intensity with time. Although the progress of

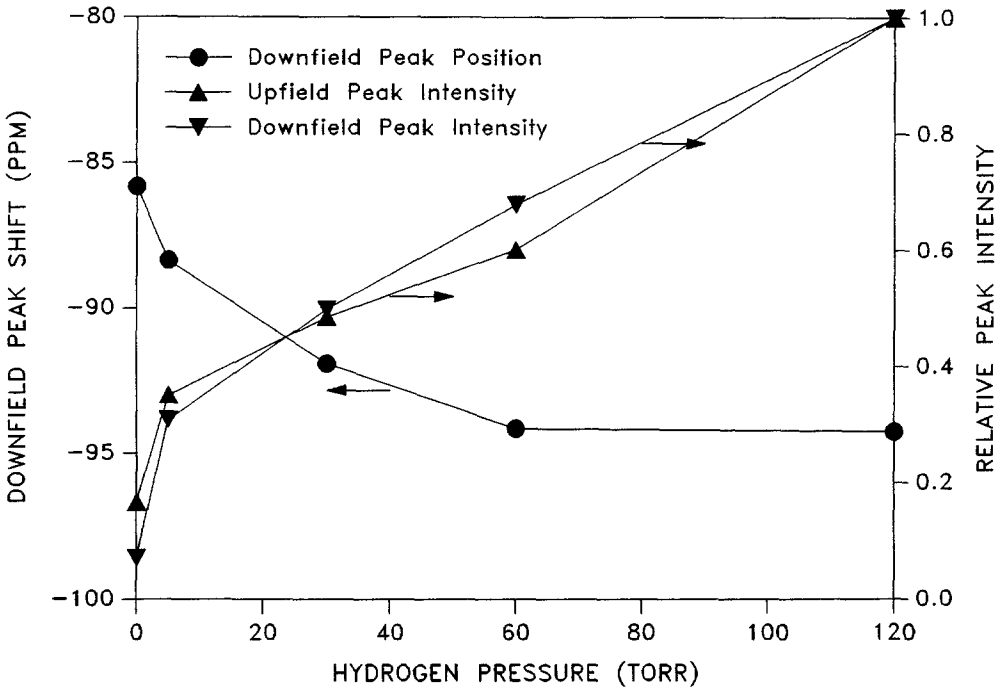

FIG. 11. Variations of the downfield peak shift and relative peak intensities with the hydrogen pressure on a Ru–Cu/SiO_2 bimetallic catalyst with 78.8 at.% Cu. Both the upfield and downfield peak intensities are normalized to that under 120 Torr hydrogen.

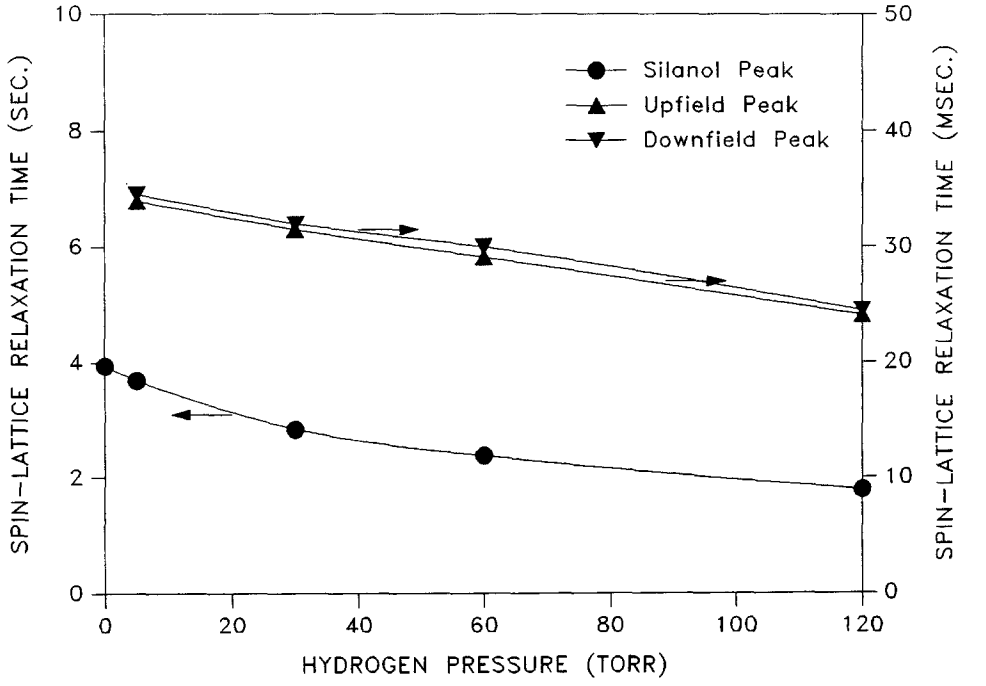

FIG. 12. Variations of the spin–lattice relaxation times for all three observed peaks with the hydrogen pressure on a Ru–Cu/SiO_2 bimetallic catalyst with 78.8 at.% Cu.

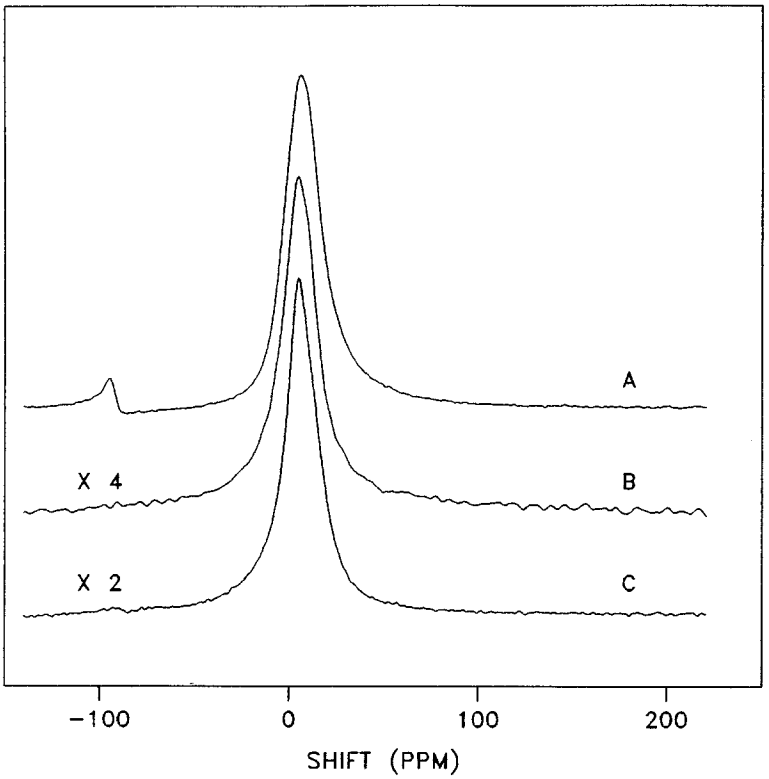

FIG. 13. NMR spectra of adsorbed hydrogen on (A) Ru–Cu/SiO_2 with 78.8 at.% Cu under 60 Torr deuterium; (B) Ru–Cu/SiO_2 with 78.8 at.% Cu, evacuated to 10^{-6} Torr for 10 min after exposure to 60 Torr deuterium; (C) 5% Cu/SiO_2 under 60 Torr deuterium. All measurements were taken after an exchange period of 24 h at 294 K.

the exchange was not closely followed, the exchange rate was comparable to that for the 4% Ru/SiO_2 catalyst (*53*). On the other hand, the irreversibly adsorbed deuterium on surfaces of the Ru–Cu bimetallic particles does not exchange with the silanol protons, as indicated by the absence of the upfield or downfield peaks in Spectrum B in Fig. 13. For a pure 5% Cu/SiO_2 catalyst sample under 60 Torr deuterium, the proton NMR spectrum (Spectrum C in Fig. 13) seems to indicate a very weak downfield peak located at about where hydrogen adsorbed on pure copper should resonate. This means that deuterium adsorbed on pure copper does exchange with the silanol proton in the silica support. This observation was confirmed on a Cu/SiO_2 catalyst with much higher copper dispersion (*44*).

DISCUSSION

Hydrogen Spillover

Hydrogen is capable of dissociative adsorption on ruthenium to produce reversibly and irreversibly adsorbed hydrogen. Once hydrogen is chemisorbed on the ruthenium surfaces it can freely migrate to adjacent copper sites. This type of spillover (from one metal site to an adjacent metal site of a different type) allows the entire surface, ruthenium and closely associated copper, to become populated with irreversibly and reversibly adsorbed hydrogen. In the present study, the Ru loading was kept constant at 4 wt% and the sample preparation conditions were identical for all catalysts. Therefore, it is reasonable to expect to have roughly the same Ru particle size

for all samples. If copper exists exclusively on the surfaces of ruthenium particles, as is often suggested for this bimetallic system (*15, 54*), then we would expect to observe a nearly constant amount of hydrogen uptake except for very high Cu loadings (Cu at.% > 50%) for which separate Cu particles are very likely to form. This effect was observed in the present work over the bulk composition range of 0 to 45 at.% Cu with a small enhancement for compositions greater than 45 at.% Cu (Fig. 6). This means that there are approximately the same total number of metal adsorption sites at surfaces of metallic and bimetallic particles to accommodate irreversibly and reversibly adsorbed hydrogen. The observation is consistent with the explanation of hydrogen spillover from ruthenium to copper. In addition, the NMR results (Fig. 4) clearly demonstrate the ability of copper to adsorb hydrogen.

It has been proposed from work on pure Ru/SiO_2 catalysts (*53*) that the reversibly adsorbed hydrogen on the surface of Ru particles is responsible for hydrogen spillover from Ru to the silica support. This concept applies directly to the $Ru–Cu/SiO_2$ system. Specifically, the reversibly adsorbed hydrogen on both Ru and Cu can spill over onto the silica support. The discrepancy between the volumetric measurements and the NMR measurements in the case of the total adsorption (Fig. 6) appears to be due partly to hydrogen spillover from the metals to the silica support. However, a major portion of this discrepancy was caused by interaction between the adsorbed hydrogen and surface Cu atoms, which in turn caused excessive line broadening. This effect will be discussed later.

The presence of copper in the bimetallic catalysts does not appear to inhibit the spillover of hydrogen from the metal particles to the silica support. The amount of reversible hydrogen and the T_1 of the silanol protons both remaining constant (Figs. 6 and 8, respectively) indicate that the amount of spiltover hydrogen on the support is not affected by copper content. However, the silanol spin–lattice relaxation time as well as hydrogen-on-metal peak intensities are dependent on hydrogen pressure because of variation in the amount of reversible hydrogen on the metals. Also, the relatively longer silanol T_1 in the case of evacuation indicates partial removal of spiltover hydrogen from the silica support.

Similar to the case of pure Ru/SiO_2 (*53*), the hydrogen–deuterium exchange on $Ru–Cu/SiO_2$ occurs only in the presence of reversible deuterium (Fig. 13, spectrum A); it does not occur in the presence of irreversible deuterium alone (Fig. 13, spectrum B). This result indicates that reversible hydrogen is responsible for hydrogen spillover from the metals to the silica support in the $Ru–Cu/SiO_2$ bimetallic system.

Hydrogen Adsorbed on Pure Cu and Ru–Cu Bimetallics

Atomic hydrogen adsorbs readily on single-crystal copper surfaces while molecular hydrogen must overcome an energy barrier of about 5 kcal/mol to achieve dissociative chemisorption (*36, 37*). Therefore, it would appear to be unlikely for molecular hydrogen to adsorb dissociatively on Cu at room temperature. The lineshift for hydrogen adsorbed on Cu/SiO_2 (−93 ppm) determined here agrees with that for hydrogen adsorbed on Cu powders (*50*). The state of hydrogen adsorbed on pure, silica-supported copper may be atomic or, perhaps, molecular. If an immobile, molecularly adsorbed hydrogen existed on copper we would expect that dipolar broadening would result in a peak on the order of 200 kHz (900 ppm) in width. Two-dimensional, random motion would reduce the apparent width by about a factor of 2. Complete narrowing of the peaks would require liquid-like, three-dimensional random motion. The observed linewidth of less than 1 kHz suggests either a liquid-like motion for a molecularly adsorbed species or a dissociatively adsorbed hydrogen unaffected by homonuclear dipole broadening.

By means of exchange of deuterium adsorbed on Cu with the silanol proton, atomic hydrogen may be introduced onto the copper surfaces. It appears that atomic hydrogen adsorbed on Cu resonates at about the same frequency (Fig. 13C) as that of hydrogen directly adsorbed on the copper surfaces. Thus the state of hydrogen adsorbed on pure Cu resembles atomic hydrogen.

The sharp line feature in the NMR spectrum for Cu/SiO_2 catalyst under 30 Torr hydrogen (Fig. 2) is a good indication of rapid motion for the adsorbed hydrogen. The same downfield peak with much broader linewidths was observed when both Ru and Cu were present (see Figs. 3, 4, and 10). The adsorbed state of hydrogen on Cu is obviously different when ruthenium is present compared to that when ruthenium is not present. In the case of pure Cu, the signal intensity for the adsorbed hydrogen was very weak and most of it was readily removed by evacuation. In the case of Ru–Cu bimetallics, the hydrogen adsorbed on Cu is perhaps less mobile, as suggested by the broader lines. Also, the signal intensities are stronger on the basis of the same amount of copper, especially for the Ru–Cu bimetallics with the highest copper loadings. The adsorbed hydrogen on Cu in the Ru–Cu bimetallics is likely to be in the atomic state since atomic hydrogen could migrate from Ru or Ru–Cu bimetallic particles to adjacent Cu particles. This same mechanism may be possible on the Ru/Cu physical mixture even though the migration path is quite long. A substantial portion of adsorbed hydrogen on copper is reversible; a portion of the adsorbed hydrogen is irreversible and bound strongly on Cu surfaces.

The nature of strongly bound hydrogen species on pure Cu (Figs. 1 and 2) is perhaps due to dissociative adsorption of hydrogen on defect-like Cu sites. The hydrogen thus adsorbed may be unable to migrate to Cu sites on low index planes because of strong bonding. The nearly identical lineshift for this hydrogen species (−88 ppm) to that for the irreversible hydrogen on pure Cu in the Ru–Cu bimetallics (−86 ppm) seems to support this postulation. Results on Cu/SiO_2 catalysts with higher copper dispersion also support this idea (*44*).

Similar to what was observed on pure Ru/SiO_2 catalysts (*53*), there are two distinct adsorbed states of hydrogen on surfaces of Ru–Cu bimetallic catalysts as well, namely, the irreversibly and the reversibly adsorbed hydrogen. On the basis of evidence from the NMR resonance linewidths, the reversibly adsorbed hydrogen on surfaces of the bimetallic particles has a higher degree of mobility than that of the irreversible hydrogen.

It was shown earlier in Fig. 5 that the resonance line for the irreversible hydrogen tended to become broader as the copper content was increased. The increased linewidth is attributed to increasing heteronuclear dipolar interaction between hydrogen and copper atoms. Both ^{63}Cu and ^{65}Cu are quadruple nuclei having a gyromagnetic ratio of 1.128 and 1.209 kHz G^{-1}, respectively, and a combined natural abundance of 100%. On the other hand, the NMR active Ru isotopes ^{99}Ru and ^{101}Ru have much smaller gryomagnetic ratios (0.144 and 0.210 kHz G^{-1}, respectively) and are less abundant (12.7 and 17.1%, respectively). The heteronuclear dipole broadening is proportional to the gyromagnetic ratio of the two nuclei involved. Hence, the effective copper–proton dipole interaction is about seven times the effective ruthenium–proton dipole interaction (for the same internuclear distance). As copper is added to the surfaces of Ru particles, the concentration of copper nuclei at the surface is increased, and increasing heteronuclear dipolar broadening is expected to occur. Assuming that the observed increase in linewidth (13.1 kHz) is caused only by this heteronuclear dipole interaction (because the homogeneous H–H dipole interaction is expected to be the same on all Ru–Cu/SiO_2 samples), and assuming that this irreversibly ad-

sorbed hydrogen on copper is relatively immobile, one can estimate the hydrogen-copper internuclear distance to be 1.4 Å. This H–Cu internuclear distance is in good agreement with the value 1.5 Å, the sum of the covalent radii for hydrogen and copper atoms.

We ascribe a major portion of the discrepancy in the amount of chemisorption between the volumetric measurements and the NMR measurements in the case of irreversible hydrogen (see Fig. 6) to shortening of the spin–spin lattice relaxation time T_2 (from 35 to 16 μs) due to increased H–Cu heteronuclear dipole interaction as Cu content is increased. The limitation from the pulse ringdown (10 μs) of the NMR receiving system prevented us from measuring the full signal intensities. As mentioned before, the amount of reversible hydrogen measured by NMR remained roughly constant. Therefore, a major portion of the discrepancy between the two techniques in the case of total adsorption was a direct consequence of the errors introduced in measurements on the irreversible hydrogen.

For the Ru–Cu/SiO_2 catalyst with 78.8 at.% Cu, the longitudinal relaxation of hydrogen adsorbed on sites corresponding to the upfield peak is similar to that of hydrogen adsorbed on pure Cu surfaces (Fig. 12). This indicates that the upfield peak represents an adsorbed hydrogen species in an environment resembling the pure Cu surfaces. It is likely to be a Cu adsorption site close to or on a Ru particle. In addition, the asymptotic behavior of the T_1 relaxation of hydrogen adsorbed on sites corresponding to the upfield peak with increasing copper content (Fig. 9) indicates an increasing deposition of copper on surfaces of ruthenium particles, reaching a complete copper coverage at very high (78.8 at.%) copper content.

The downfield shift for the hydrogen reversibly adsorbed on bimetallic particles (from 62 to 49 ppm for Ru; see Fig. 7) was an effect solely due to addition of copper. Previous work has demonstrated that the variation of this peak is due to the fast exchange of adsorbed hydrogen to and from copper and ruthenium environments (*40*). The asymptotic behavior of this shift extrapolates to a value of 49 ppm at 78.8 at.% Cu corresponding to reversibly adsorbed hydrogen on copper very close to or on the ruthenium particles. From the difference in these lineshifts, it is estimated that the fast-exchange frequency for the reversible hydrogen between Ru and Cu-on-Ru sites is at least 3 kHz at room temperature. Since no fast exchange between hydrogen adsorbed on pure Cu sites (downfield peak) and hydrogen adsorbed on Cu-on-Ru sites (upfield peaks) was observed, the fast-exchange frequency should be less than the frequency difference between these two resonances, or 31 kHz.

It is interesting to note that resonance line for the hydrogen adsorbed on copper close to or on ruthenium appears upfield instead of downfield with respect to the reference shift. The downfield resonance line for the hydrogen adsorbed on pure Cu sites may be attributed to Knight shift interaction by the 4*s* conduction electrons in copper (*50*). On the other hand, the upfield resonance line for the hydrogen adsorbed on pure Ru sites may be due to Knight shift interaction by the 4*d* conduction electrons via an opposite spin polarization. One possible explanation for the observed shift is that the sublayer Ru atoms have a stronger spin polarization effect on the adsorbed hydrogen than the overlayer Cu atoms. Another possible explanation invokes a minor electronic perturbation on the Cu 3*d* electrons by the Ru 4*d* conduction electrons, and the perturbed Cu 3*d* electrons would exert a stronger spin polarization on the adsorbed hydrogen than the Cu 4*s* electrons. The second explanation seems to agree with a theoretical calculation (*55*) and experimental UPS results (*24, 34*).

Surface Composition

The influence of copper on the lineshift of the reversibly adsorbed hydrogen may be

used as a measure of surface composition for the Ru–Cu bimetallic catalysts. In the fast exchange limit, the observed lineshift is the average lineshift of reversible hydrogen on the two adsorption sites weighted by the relative population of these two adsorption sites. When all adsorption sites are filled, it is expressed as

$$\delta_{obs} = X_{Ru}\,\delta_{Ru} + X_{Cu}\,\delta_{Cu},$$

where δ_{obs} is the observed lineshift for the reversible hydrogen on the Ru–Cu bimetallics; δ_{Ru} and δ_{Cu} are lineshifts for the reversible hydrogen on Ru and Cu deposited on Ru, respectively; X_{Ru} and X_{Cu} are surface fractions of Ru and Cu, respectively. Since the sum of X_{Ru} and X_{Cu} is unity, the surface fraction of Ru may be expressed in terms of lineshifts as follows:

$$X_{Ru} = (\delta_{obs} - \delta_{Cu})/(\delta_{Ru} - \delta_{Cu}).$$

Hence, the shift values shown in Fig. 7 can then be readily used to compute surface compositions.

Figure 14 shows the trend for the surface fraction of Ru as a function of the bulk copper composition expressed in atomic percent. As can be seen, X_{Ru} falls quickly as the overall composition is increased from 0 to 20 at.% Cu. It begins to level off at about 35 at.% Cu and approaches zero at 78.8 at.% Cu, where complete masking of the surfaces of Ru particles by Cu was assumed to occur.

Also shown in Fig. 14 is the surface composition of ruthenium in the bimetallic particles under the assumption that all the copper resides at the surface in a single monolayer. For the particles, all with a dispersion of about 29% (as determined from the irreversible hydrogen uptake shown in Fig. 6 assuming a stoichiometric ratio of one for both $H_{(irr)}/Ru_{(s)}$ and $H_{(irr)}/Cu_{(s)}$), a monolayer of copper will completely cover

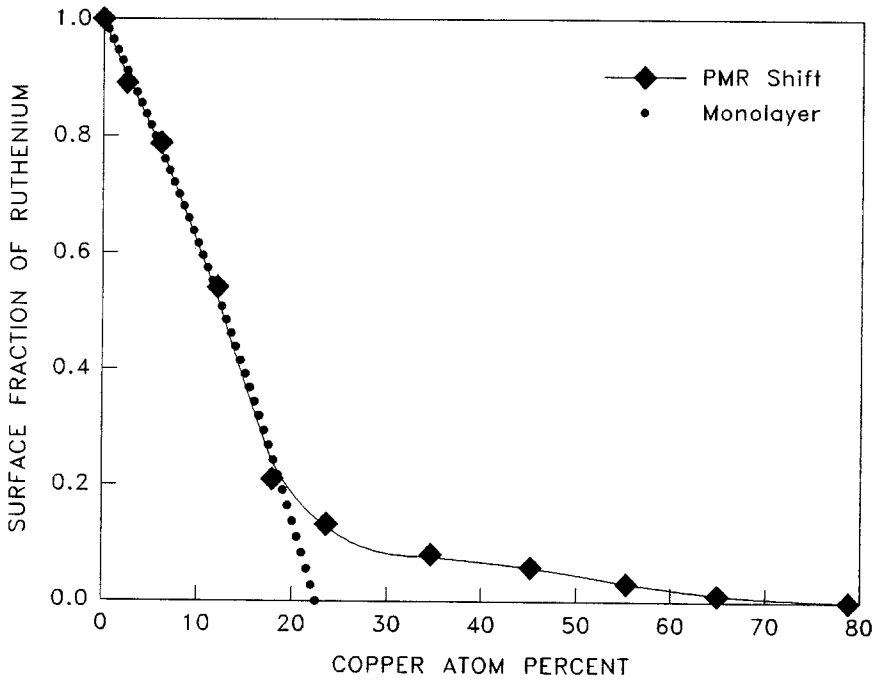

FIG. 14. Plot of surface fraction of ruthenium as a function of the copper content for a series of Ru–Cu/SiO_2 bimetallic catalysts. The Ru surface fraction is calculated from the observed upfield NMR lineshift corresponding to the reversible hydrogen. The Ru surface fraction corresponding to a monolayer growth of Cu on Ru is also shown for comparison.

the surface at an overall copper composition of 22.5 at.%. The monolayer assumption and the surface composition determined from NMR agree very well up to a copper content of about 18 at.%; this agreement indicates the copper does tend to cover the ruthenium particles in a thin layer until a complete monolayer is nearly formed. At an overall copper content of 18.5 at.% (surface coverage of 78.3 at.% copper) copper islands, separate copper particles, or both begin to form. A complete coverage of the Ru surface by Cu can be obtained only at very high Cu loadings. This view was justified by the emergence of the downfield peak (see Fig. 4), which represents hydrogen adsorbed on bulk copper.

Surface composition is the most important parameter in characterization of Ru–Cu bimetallic catalysts. The ability to measure surface composition allows calculation of turnover frequencies for various catalytic reactions, which in turn provides valuable insight into the catalytic nature of these bimetallic catalysts.

CONCLUSIONS

Both hydrogen chemisorption and NMR of adsorbed hydrogen indicate hydrogen spillover from Ru to Cu. From NMR measurements, it is indicated that pure Cu is capable of adsorbing hydrogen. There are two adsorbed states of atomic hydrogen on surfaces of bimetallic particles in the Ru–Cu/SiO_2 catalysts: irreversibly and reversibly adsorbed states. The reversible hydrogen is more mobile than the irreversible hydrogen. The surface compositions of the Ru–Cu bimetallic catalysts can be obtained from the NMR resonance lineshifts associated with rapid exchange of the reversibly adsorbed hydrogen at the surface. Copper atoms preferentially segregate to the surface of the bimetallic particles and in so doing cover the ruthenium in nearly a monolayer fashion. The formation of three-dimensional Cu islands and pure Cu particles is possible at high Cu surface coverages.

ACKNOWLEDGMENT

This work was supported by the U.S. Department of Energy, Office of Basic Energy Sciences, Contract W-7405-ENG-82. The support of the Engineering Research Institute of Iowa State University is also acknowledged.

REFERENCES

1. Sinfelt, J. H., Barnett, A. E., and Carter, J. L., US Patent 3,617,518, Nov. 2, 1971.
2. Sinfelt, J. H., *J. Catal.* **29,** 308 (1973).
3. Prestridge, E. B., Via, G. H., and Sinfelt, J. H., *J. Catal.* **50,** 115 (1977).
4. Sinfelt, J. H., *Acc. Chem. Res.* **10,** 15 (1977).
5. Rouco, A. J., Haller, G. L., Oliver, J. A., and Kemball, C., *J. Catal.* **84,** 297 (1983).
6. Haller, G. L., Resasco, D. E., and Wang, J., *J. Catal.* **84,** 477 (1983).
7. Hong, A. J., Rouco, A. J., Resasco, D. E., and Haller, G. L., *J. Phys.Chem.* **91,** 2665 (1987).
8. Hong, A. J., McHugh, B. J., Bonneviot, L., Resasco, D. E., Weber, R. S., and Haller, G. L., *in* "Proceedings, 9th International Congress on Catalysis, Calgary 1989" (M. J. Phillips and M. Terman, Eds.), pp. 1198–1205. Chem. Institute of Canada, Ottawa, 1988.
9. Shastri, A. G., Schwank, J., and Galvagno, S., *J. Catal.* **100,** 466 (1986).
10. Damiani, D. E., Derez Millan, E. D., and Rouco, A. J., *J. Catal.* **101,** 162 (1986).
11. Bond, G. C., and Turnham, B. D., *J. Catal.* **45,** 128 (1976).
12. Bond, G. C., and Yide, X., *J. Mol. Catal.* **25,** 141 (1984).
13. Lai, S. Y., and Vickerman, J. C., *J. Catal.* **90,** 337 (1984).
14. Schoenmaker-Stolk, M. C., Verwijs, J. W., and Scholten, J. J. F., *Appl. Catal.* **30,** 339 (1987).
15. Sinfelt, J. H., Lam, Y. L., Cusumano, J. A., and Barnett, A. E., *J. Catal.* **42,** 227 (1976).
16. Helms, C. R., and Sinfelt, J. H., *Surf. Sci.* **72,** 229 (1978).
17. Christmann, K., Ertl, G., and Shimizu, H., *J. Catal.* **61,** 397 (1980).
18. Shimizu, H., Christmann, K., and Ertl, G., *J. Catal.* **61,** 412 (1980).
19. Vickerman, J. C., Christmann, K., and Ertl, G., *J. Catal.* **71,** 175 (1981).
20. Vickerman, J. C., and Christmann, K., *Surf. Sci.* **120,** 1 (1982).
21. Vickerman, J. C., Christmann, K., Ertl, G., Heiman, P., Himpsel, F. J., and Eastman, D. E., *Surf. Sci.* **134,** 367 (1983).
22. Christmann, K., and Ertl, G., *J. Mol. Catal.* **25,** 30 (1984).
23. Brown, A., and Vickermann, J. C., *Surf. Sci.* **140,** 261 (1984).

24. Richter, L., Bader, S. D., and Brodsky, M. B., *J. Vac. Sci. Technol.* **18,** 578 (1981).
25. Bader, S. D., and Richter, L., *J. Vac. Sci. Technol. A* **1,** 1185 (1983).
26. Yates, J. T., Jr., Peden, C. H. F., and Goodman, D. W., *J. Catal.* **94,** 576 (1985).
27. Paul, J., and Hoffman, F. M., *Surf. Sci.* **172,** 151 (1986).
28. Houston, J. E., Peden, C. H. F., Blair, D. S., and Goodman, D. W., *Surf. Sci.* **167,** 427 (1986).
29. Park, C., Bauer, E., and Poppa, H., *Surf. Sci.* **187,** 86 (1987).
30. Hansen, M., "Constitution of Binary Alloys," 2nd ed., p. 620. McGraw–Hill, New York, 1958.
31. Sinfelt, J. H., Via, G. H., and Lytle, F. W., *J. Chem. Phys.* **72,** 4832 (1980).
32. Peden, C. H. F., and Goodman, D. W., *in* "Catalyst Characterization Science: Surface and Solid State Chemistry," ACS Symp. Ser. No. 288, pp. 185–198. American Chemical Society, Washington, DC, 1985.
33. Kim, K. S., Sinfelt, J. H., Eder, S., Markert, K., and Wandelt, K., *J. Phys. Chem.* **91,** 2337 (1987).
34. Houston, J. E., Peden, C. H. F., Feibelman, P. J., and Hamann, D. R., *Phys. Rev. Lett.* **56,** 375 (1986).
35. Smale, M. W., and King, T. S., *J. Catal.* **119,** 441 (1989).
36. Balooch, M., Cardillo, M. J., Miller, D. R., and Stickney, R. E., *Surf. Sci.* **46,** 358 (1974).
37. Greuter, F., and Plummer, E. W., *Solid State Commun.* **48,** 37 (1983).
38. Goodman, D. W., Yates, J. T., Jr., and Peden, C. H. F., *Surf. Sci.* **164,** 417 (1985).
39. Goodman, D. W., and Peden, C. H. F., *J. Catal.* **95,** 321 (1985).
40. King, T. S., Wu, X., and Gerstein, B. C., *J. Amer. Chem. Soc.* **108,** 6056 (1986).
41. Narita, T., Miura, H., Sugiyama, K., Matsuda, T., and Gonzalez, R. D., *J. Catal.* **103,** 492 (1987).
42. Lu, K., and Tatarchuk, B. J., *J. Catal.* **106,** 166 (1987).
43. Lu, K., and Tatarchuk, B. J., *J. Catal.* **106,** 176 (1987).
44. Wu, X., Gerstein, B. C., and King, T. S., to be published.
45. Cheung, T. T. P., Worthington, L. E., Murphy, P. D. B., and Gerstein, B. C., *J. Magn. Reson.* **41,** 158 (1980).
46. Fry, C. G., Iwamiya, J. H., Apple, T. M., and Gerstein, B. C., *J. Magn. Reson.* **63,** 214 (1985).
47. Gerstein, B. C., "Alternating Circuit Theory and Pulsed NMR," IS-49244C-13. Available from NTIS, US Dept. of Commerce, 5265 Port Royal Road, Springfield, VA 22161
48. Stoll, M. E., "A Fast Recovery, Low Noise Receiver–Amplifier for Pulsed NMR Experiments." SAND80-8797, Sandia National Laboratory, 1980.
49. King, T. S., Goretzke, W. J., and Gerstein, B. C., *J. Catal.* **107,** 583 (1987).
50. Ito, T., and Kadowaki, T., Japan. *J. Appl. Phys.* **14,** 1673 (1975).
51. Shield, L. S., and Russell, W. W., *J. Phys. Chem.* **64,** 1592 (1960).
52. Rossington, D. R., and Holden, S. J., *Nature (London)* **199,** 589 (1963).
53. Wu, X., Gerstein, B. C., and King, T. S., *J. Catal.* **118,** 238 (1989).
54. Wu, X., Smale, M. W., Gerstein, B. C., and King, T. S., AIChE Annual Meeting, New York, November 1987, Paper No. 15a.
55. Ma, C. Q., Ramana, M. V., and Copper, B. R., *J. Vac. Sci. Technol. A* **1,** 1095 (1983).